

---

# FOUNDATION MODELS FOR STRUCTURAL HEALTH MONITORING

---

A PREPRINT

**Luca Benfenati**  
DAUIN, Politecnico di Torino  
Turin, 10125  
luca.benfenati@polito.it

**Daniele Jahier Pagliari**  
DAUIN, Politecnico di Torino  
Turin, 10125  
daniele.jahier@polito.it

**Luca Zanatta**  
DEI, University of Bologna  
Bologna, 40136  
luca.zanatta3@unibo.it

**Yhorman Alexander Bedoya Velez**  
DAUIN, Politecnico di Torino  
Turin, 10125  
s287296@studenti.polito.it

**Andrea Acquaviva**  
DEI, University of Bologna  
Bologna, 40136  
andrea.acquaviva@unibo.it

**Massimo Poncino**  
DAUIN, Politecnico di Torino  
Turin, 10125  
massimo.poncino@polito.it

**Enrico Macii**  
DIST, Politecnico di Torino  
Turin, 10125  
enrico.macii@polito.it

**Luca Benini**  
D-ITET, ETH Zurich  
Zürich, 8092  
lbenini@iis.ee.ethz.ch

**Alessio Burrello**  
DIST, Politecnico di Torino  
Turin, 10125  
alessio.burrello@polito.it

## ABSTRACT

Structural Health Monitoring (SHM) is a critical task for ensuring the safety and reliability of civil infrastructures, typically realized on bridges and viaducts by means of vibration monitoring. In this paper, we propose for the first time the use of Transformer neural networks, with a Masked Auto-Encoder architecture, as *Foundation Models* for SHM. We demonstrate the ability of these models to learn generalizable representations from multiple large datasets through self-supervised pre-training, which, coupled with task-specific fine-tuning, allows them to outperform state-of-the-art traditional methods on diverse tasks, including Anomaly Detection (AD) and Traffic Load Estimation (TLE). We then extensively explore model size versus accuracy trade-offs and experiment with Knowledge Distillation (KD) to improve the performance of smaller Transformers, enabling their embedding directly into the SHM edge nodes.

We showcase the effectiveness of our foundation models using data from three operational viaducts. For AD, we achieve a near-perfect 99.9% accuracy with a monitoring time span of just 15 windows. In contrast, a state-of-the-art method based on Principal Component Analysis (PCA) obtains its first good result (95.03% accuracy) only considering 120 windows. On two different TLE tasks, our models obtain state-of-the-art performance on multiple evaluation metrics ( $R^2$  score, MAE% and MSE%). On the first benchmark, we achieve an  $R^2$  score of 0.97 and 0.85 for light and heavy vehicle traffic, respectively, while the best previous approach stops at 0.91 and 0.84. On the second one, we achieve an  $R^2$  score of 0.54 versus the 0.10 of the best existing method.

**Keywords** Structural Health Monitoring · Traffic Load Estimation · Foundation Models · Masked Autoencoders · Deep Learning

## 1 Introduction

Structural Health Monitoring (SHM) is crucial to ensure the longevity and safety of critical infrastructures such as bridges, highways, and tunnels. In fact, these structures are subject to deterioration due to factors such as ageing, environmental conditions, and traffic loads, posing potential safety hazards and substantial financial burdens for maintenance and repairs.

SHM systems address this challenge by proactively and continuously monitoring infrastructure in real time, enabling early detection of anomalies and potential damages. This facilitates timely interventions that ensure public safety while optimizing resource allocation through cost-effective strategies. When applied to critical infrastructures such as bridges and viaducts, SHM can also exploit Traffic Load Estimation (TLE) as a metric that captures the dynamic nature of traffic loads that the structures endure, to continuously assess structural health and predict maintenance needs.

A typical SHM system comprises a network of sensors responsible for measuring multiple parameters relevant to the current state of the structure as well as its surrounding environment. The most widely used SHM sensing devices include fiber optic sensors [1, 2, 3, 4], accelerometers [5, 6], cameras [7] and strain gauges [8]. Among these options, networks of Micro-Electro-Mechanical Systems (MEMS) for vibration monitoring stand out due to their cost-effectiveness and relatively simple deployment in diverse environments. Data gathered by these accelerometers are then used as the input of a Machine Learning (ML) model to address tasks such as AD or TLE. These devices have demonstrated high accuracy compared to other technologies on several SHM tasks [9].

ML approaches for vibration-based SHM span a diverse range of techniques, from classic methods as in [10, 11], to more recent deep learning solutions such as Convolutional Neural Networks (CNNs) [12] and Autoencoders [13, 14, 15]. While Transformer neural networks have revolutionized the Computer Vision and Natural Language Processing (NLP) fields, in SHM they have only been applied to camera-based monitoring solutions [16], and not yet (to our knowledge) to vibration-based ones. Furthermore, existing literature primarily focuses on models tailored to single tasks, like AD or TLE, and does not consider the possibility of developing a unified, foundation approach capable of addressing multiple SHM challenges with a single ML model.

In this paper, we introduce two key contributions to acceleration-based SHM. We consider for the first time the application of Transformers this task, using a Masked Autoencoder architecture inspired by [17]. Furthermore, building on the recent breakthroughs of foundation models across diverse domains (language, vision, etc..) [18], we explore *self-supervised learning* to develop models that learn generalizable representations of acceleration data for SHM, and can be then fine-tuned to perform multiple diverse tasks with high performance, including AD and different forms of TLE. This work demonstrates the potential of foundation models for advancing data-driven SHM, especially to cope with the difficulty of collecting large amounts of labelled data, which requires time-consuming and costly instrumentations of the target infrastructure with other types of sensors, such as cameras or Weigh-in-Motion (WiM) [19] systems to obtain ground truths.

In summary, the contributions of this work are:

- We consider three different SHM datasets, including a newly collected one, larger than those introduced in previous works and fully labelled.
- We build a Transformer-based Masked Autoencoder inspired by [17] to test if a foundation model approach could outperform individual task-specific models on SHM tasks. By pre-training on all three datasets without using labels (self-supervised learning) and then fine-tuning on each specific task, we achieve better results than training three separate models from scratch. Notably, although all our datasets are labelled, this 2-stage training protocol only uses supervision signals during fine-tuning, simulating the availability of large amounts of unlabelled samples (much easier to collect in practice) and a relatively smaller amount of labelled ones.
- Through our experiments, our fine-tuned models outperform state-of-the-art algorithms on all three datasets. In particular, on the first dataset, we achieve an AD accuracy of 99.92%, a sensitivity of 100%, and a specificity of 99.9%, with respect to state-of-the-art 75.76%, 55.68%, and 98.75%. On the other two datasets, and on three TLE variants, we achieve an  $R^2$  score of 0.97, 0.85, and 0.54 respectively, outperforming the state-of-the-art that stops at 0.91, 0.84, and 0.10.
- We carry out an extensive search on the optimal model size. In this context, we test Knowledge Distillation (KD) to train smaller models to imitate larger ones, ultimately targeting deployment on resource-constrained nodes for real-time SHM at the edge. Results show that distilled models often outperform standardly fine-tuned and equally sized counterparts on downstream tasks.

The rest of the paper is organized as follows. Section 2 provides the necessary background. Section 3 overviews the SHM literature, describing the different approaches to AD and TLE. Section 4 describes the three considered viaducts, the corresponding SHM sensor networks, and the data acquisition and labeling processes. Section 5 details our foundation model approach, presenting the processing pipeline, the architecture of the model, and its training procedure. Section 6 presents the experimental results and Section 7 concludes the paper. We open-source our code and pre-trained models at <https://github.com/eml-eda/tle-supervised>.

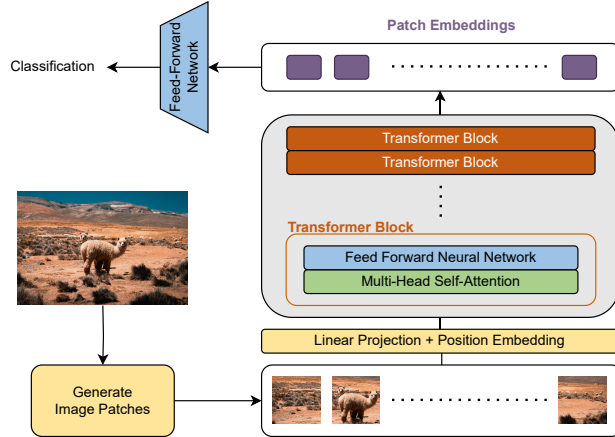


Figure 1: Vision Transformer ViT Architecture

## 2 Background

### 2.1 Transformer Neural Networks

The Transformer architecture was introduced in 2017 [20], ushering in a new era for NLP applications and DL in general. The architecture leverages an encoder-decoder structure with stacked self-attention and feedforward layers, enabling the model to process input sequences and generate outputs (e.g., translations) autoregressively. Its core innovation lies in self-attention, which allows the model to directly attend to relevant parts of the input sequence, capturing long-range dependencies. Scaled dot-product and Multi-Head Self-Attention (MHSA) enable efficient and diverse attention computation, while positional encodings address the lack of inherent sequence awareness [21]. Its impact goes beyond NLP, making it a cornerstone of modern DL due to its scalability, parallelizability, and ability to model long-range dependencies. In our work, we use an architecture derived from the Vision Transformer (ViT) [22], which first applied an attention-based Transformer to image processing. This is achieved by breaking the image into fixed-size patches, linearly embedding each of them, adding the position embeddings and then feeding the resulting sequence of vectors to a standard Transformer encoder. A simplified scheme of a ViT encoder architecture is shown in Figure 1. Notably, we apply a similar architecture to vibration data rather than standard RGB images, after extracting their spectrogram, as detailed in Sec. 5.1.

### 2.2 Masked Autoencoders

Masked autoencoders sparked renewed interest in 2021 when [23] successfully adopted them as scalable self-supervised learners for Computer Vision applications. They are encoder-decoder models, whose encoder is the ViT shown in the previous section. The decoder, instead, takes the patch embeddings as inputs and is tasked to reconstruct the original image. During training, some image patches are randomly masked before being fed to the network, forcing the autoencoder to reconstruct the missing information solely from the remaining visible parts. This process encourages the model to learn robust and diverse representations of visual features. The simplicity and effectiveness of this scheme have led masked autoencoders to achieve state-of-the-art performance in various downstream tasks, demonstrating their potential as powerful tools for visual representation learning [21]. The specific masked autoencoder architecture used in our work will be detailed in Sec. 5.2 and shown in Fig. 4.

### 2.3 Foundation Models

The term Foundation Model refers to a DL model that is trained on broad data, using self-supervision at scale, and can be adapted to a wide range of downstream tasks [18]. The pre-training phase is usually carried out on diverse and unlabelled data, to produce general-purpose data representations that, unlike specialized models trained for specific tasks, serve as a foundational block. Fine-tuned on specific downstream tasks, foundation models offer several advantages: increased training efficiency, broader applicability, and the ability to transfer learned knowledge across domains. This shift in AI from task-specific models to a reusable “foundation” approach has opened new avenues for leveraging the power of DL across various applications, from tasks like summarization and translation in NLP[24] to image classification and

object detection in Computer Vision [25, 26], and time-series forecasting [27, 28]. However, the adoption of this novel paradigm in other domains, including SHM, is still unexplored.

### 3 Related Works

This section presents the current state-of-the-art approaches to SHM, including both AD (Sec. 3.1) and TLE (Sec. 3.2). For each task, we first broadly overview works that use other sensors, and then focus on accelerometer-based methods.

#### 3.1 Anomaly Detection

Concerning visual AD, in [16], a ViT-like approach is applied to the semantic segmentation of images to identify damaged structural components in a railway viaduct. This approach outperforms existing vision-based methods by a significant margin with 97% and 90% mean Intersection Over Union (mIoU) for component and damage segmentation respectively. [29] proposes a solution for detecting damage on a bridge from displacement measurements using a roving multi-camera vision system. Five unsupervised AD techniques are compared (Autoencoder, K-Nearest Neighbours, Kernel Density, Local Outlier Factor and Isolation Forest), achieving an F1 score that ranges from 0.96 to 0.97 across a series of controlled laboratory tests.

Another line of work [30] proposed a charging scheduling to replenish a wireless rechargeable sensor network for bridge monitoring by an unmanned aerial vehicle (UAV).

However, most AD methods for SHM rely on acceleration data. In [31], the authors use a 1-dimensional CNN to estimate the Probability of Damage, evaluating nine scenarios of increasing damage severity. Similarly, [12] proposes a CNN for multiclass unbalanced AD. They first extract statistical features from acceleration data (i.e. maximum, minimum, mean, variance, skewness, kurtosis), which are then used as the input of 3 stacked convolutional blocks, followed by global average pooling and softmax to predict the category of the damage, choosing from seven distinct anomalies. This method achieves an overall accuracy of 97.6% on a real-world dataset of a long-span cable-stayed bridge in China. In [32, 33], the authors explore spiking neural networks to accurately classify the damage in a viaduct, achieving an accuracy of 95% and Matthew’s correlation coefficient (MCC) values of 0.88.

All aforementioned approaches utilize supervised learning, which requires both healthy and damaged samples for training. In contrast, the authors of [34] employ an Autoencoder for indirect damage diagnosis in a simulated bridge environment, extracting representative features from vehicles’s vibration response, which are then used for an unsupervised damage severity comparison model and a semi-supervised damage severity estimation model. When predicting the damage severity in a range of 30 possible levels, their predicted level is off by 5 levels on average with respect to the ground truth. In [35], an unsupervised learning method for Recurrent Neural Network (RNN) is employed to detect and identify structural damage, achieving 93% and 85% accuracy for detection and localization. The dataset used for this study was obtained through simulations rather than from a real-world bridge.

Lastly, [36] is the most recent and promising approach for AD on vibration data. It is based on Principal Component Analysis (PCA) compression and does not require labelled anomalies. Specifically, the PCA coefficients are fitted only on healthy data. Then, anomalous vibrations associated with damages, being out-of-distribution samples, will be poorly reconstructed from principal components extracted with those coefficients. Accordingly, this AD scheme classifies all samples with a PCA reconstruction error higher than a threshold as anomalies. On one of the datasets we use, collected from a real-world viaduct located in northern Italy on a state highway, they can reach 98.8% accuracy, 100% specificity, and 97.33% sensitivity on the anomaly detection task. In Section 6, we consider this last method as the state-of-art to compare with.

#### 3.2 Traffic Load Estimation

Kamkar et al. [7] use smart cameras to detect, classify, and quantify vehicles on public bridges, achieving a notable accuracy of 92.1% in high-traffic scenarios. However, the system’s performance decreased substantially to 74.8% when faced with reduced lighting conditions on the bridge. This finding emphasizes how visual-based methods are sensitive to environmental factors, particularly lighting, which can impact their overall dependability. An alternative method, as illustrated in [37, 38], employs magnetic sensors paired with adaptive thresholds and classification trees. This approach demonstrates varying levels of accuracy, ranging from 84.7% to 99.9%, depending on the traffic conditions analyzed. Notably, in [37], the authors achieve the highest precision in a testing scenario that involves a single vehicle, consistently moving at a slow speed, which does not reflect real-world traffic conditions. In [2, 3, 4], the authors investigate alternative sensor technologies, including fiber optic sensors and infrared sensors, for vehicle detection and classification. These technologies demonstrate the potential to achieve accurate results; however, they may encounter

challenges related to sensitivity to environmental factors as well as higher installation costs that could hinder their widespread implementation outside urban environments. For example, deploying single roadside-installed sensor fiber strips might not be feasible in less populated areas. The work of [39] develops an agent that uses TLE information to efficiently control traffic signals based, adjusting speed profiles for approaching vehicles to smooth traffic flows.

Very few works use acceleration data for TLE. In [40], authors showcase the superiority of MEMS accelerometers, proving them to be insensitive to sensor placement and robust to the potential presence of damage in the bridge. In [41], the TLE problem based on SHM sensors was framed as an anomaly detection problem, where vibration patterns that deviated from a periodically updated baseline were associated with the passage of a vehicle. This method is interesting because it does not rely on labelled data, but the overall performance is not sufficient in high-traffic conditions. They use k-means clustering to distinguish 2 groups of vehicles (light and heavy), obtaining in low traffic load conditions extracted features that are significantly different between the two groups, thus resulting in a p-value  $< 0.0001$ . [10] is the most recent work on TLE with accelerometer data. It compares several classic machine learning approaches, such as Linear Regressor, Random Forest, k-nearest Neighbors, Support Vector Regressor, and a deep learning approach based on Multi-Layer Perceptron, using data from MEMS accelerometers, achieving state-of-the-art performance with an  $R^2$  of 0.91 on light vehicles and 0.84 on heavy vehicles. This is the method that we compare with in Section 6.

## 4 Structural Health Monitoring Installations and Datasets

Table 1: Information about the use cases’ dataset. Abbreviations: AD: anomaly detection, TLE: traffic load estimation.

	Task	N. of Samples [Train / Test]	Time [Train / Test]	Data Dimension	Data Stride	N. of Sens.	Label
UC1	AD	302.4k / (172.8k N., 172.8k A.)	7d / (4d N., 4d A.)	5s $\times$ 100Hz	2s $\times$ 100Hz	1	Normal / Anomaly
UC2	TLE	651 / 279	21:42 / 9:18 min:sec	60s $\times$ 100Hz	2s $\times$ 100Hz	1	# of Light/Heavy Vehicles
UC3	TLE	699.9k / 50k	36 hours / 6 hours	60s $\times$ 100Hz	15s $\times$ 100Hz	142	# of Vehicles

This section describes the three SHM use cases considered in our work.

### 4.1 Use Case 1 (UC1): Anomaly Detection Task

The first use case exploits the vibration data collected on a dual-carriageway state highway located in northern Italy. The two carriageways are on two independent viaducts, composed of 9 different sections each. In 2019, one of the spans of the viaducts underwent a technical intervention to strengthen the structure, which caused a change in the vibration signal collected. Before the intervention, this section was instrumented with five SHM nodes, directly placed under the bridge to monitor viaduct vibration. Therefore, vibration data from both before and after the intervention were gathered from the sensors. These data are used in this study as a proxy for an abrupt change in the viaduct structure caused, for example, by external factors such as an earthquake. Namely, we consider vibrations raw data collected *after* the intervention as the normal data produced by a “sane” viaduct, while the accelerations measured *before* the intervention as the “anomaly”, given the high degradation of the bridge’s structure. Sensor nodes for vibration monitoring in this installation use the LIS344ALH analog 3-axial accelerometer [42] with a full-scale range of  $\pm 2 / \pm 6g$ , that gather vibration data in the three directions, x, y, z, with an angle of  $90^\circ \pm 2\%$  between each other. The system also includes an HTS221 temperature and humidity sensor [43], and an STM32L476VGTx microcontroller as a computational core, used for data analytics tasks and the scheduling of the data collection steps. The microcontroller unit is an ARM 32-bit Cortex-M4 running at 80 MHz, with 96 KB of SRAM and 1MB of Flash memory.

**Dataset** The employed dataset is the same described in [36], comprising a total of 15 days of continuous monitoring of the viaduct. For our analysis, we consider only the central sensor of the chain, which is the one most influenced by the viaduct vibration. The data include measurements from 4 days before the maintenance intervention, labeled as anomalies, and two intervals of 4 and 7 days respectively, after the intervention, labeled as normal data. We select as the test set the two intervals of 4 days to have a perfect balance between anomalies and normal data. The remaining 7 days of normal data are used to train the AD algorithm. Note that anomalies are not used during training given that, for this task, we only consider one-class models trained to identify anomalies as outliers. The latter are, therefore, used only at test time to assess the detection accuracy.

### 4.2 Traffic Load Estimation Task

#### 4.2.1 Use Case 2 (UC2)

As a first benchmark for TLE, we consider another viaduct located in Italy, equipped with a SHM sensor network since 2017. A view of the viaduct and of the installed sensors is given in Fig. 2. The viaduct is sustained by five concrete



Figure 2: A) Aerial view of the viaduct under analysis. B) Sensor positioning on prestressing cables. C) Prestressing cables.

pillars and has a total length of  $\sim 580$  m. The spans are 67 m-112 m long. Each span is formed by a steel caisson inside which there are 12 prestressing cables. The height of the cross-section of the main beam varies from 6.0 m (at the bearings) to 3.0 m (at the center line of each span). After the construction, a series of unbound tendons (27 strands each) were placed, prestressed, and anchored to the abutments. Since the structural safety of a prestressed bridge is highly dependent on the durability of these cables, a system of sensors (see Fig. 2) has been installed on them to check for breakages. Since September 2017, the sensor network has been fully active and is gathering data stored in the cloud. The network comprises 90 sensors that gather data from all the spans positioned in the upper part of the pre-stressed cables. Each node comprises an STM32F405RG microcontroller (MCU), which takes care of managing the data acquisition and optionally performs simple data analytics steps, and the same accelerometer, temperature and humidity sensors described in Section 4.1.

**Dataset** We consider the data of a single section, specifically section 10, which corresponds to the area of the road in which an optical camera has been installed for the labelling process, i.e., to compute the ground truth reference for TLE. This section comprises 7 sensors, mounted on different tendons. Our study uses only the central one, which experiences the highest vibrations. In detail, we consider 31 minutes of recorded accelerator from the z-axis of the sensor and a synced video from the camera. Train and test data are obtained considering a 70:30 split ratio: training data consists of 21 minutes and 42 seconds, while the other 9 minutes and 18 seconds are used for testing. Data were collected between 8.00 a.m. and 9.00 a.m., with the camera working at 10 Frames Per Second (FPS). Labels were extracted from the video assigning value 1 to acceleration samples corresponding to each camera frame in which a light vehicle crossed an ideal vertical line placed above the pillar of section 10, and value 2 for each crossing by a heavy vehicle. Value 0 was associated to frames without crossing vehicles. Noteworthy, given the sampling frequency of the camera (10 FPS) and accelerometer (100 Hz), slices of 10 consecutive acceleration samples always receive the same label. Acceleration data and labels were then synchronized to form a single multi-variate time series dataset, with  $100 \times 1860s$  (i.e., 31 minutes  $\times 60$ ) samples. The final TLE label was computed as the sum of the 1s and 2s in the window divided by 10, as in [10] (details in Sec. 5.1).

#### 4.2.2 Use Case 3 (UC3)

The third case study involves a roadway bridge during normal operation. The bridge consists of 18 spans and is 583 meters long, with two lanes. It is a reinforced concrete girder bridge with an isostatic static scheme. Each span is 20 meters long, except for the first and last, which are 10 and 29.5 meters long, respectively. An industrial SHM system has been recording data since the beginning of 2022. It includes 282 MEMS biaxial inclinometers and 142 MEMS triaxial accelerometers with a  $\pm 2g$  full scale and 100 Hz sample rate. They are evenly distributed across spans, with accelerometers monitoring the two external beams in each span. Three sensors are installed for each beam at the quarter, third, and midspan positions.

In addition to the monitoring system, a WiM system is located about 600 meters before the viaduct. This section does not have any highway exits or parking areas. The WiM system provides a different source for ground truth data for the study, compared to Use Case 2. Namely, it offers detailed information about the traffic on the bridge, including the lane

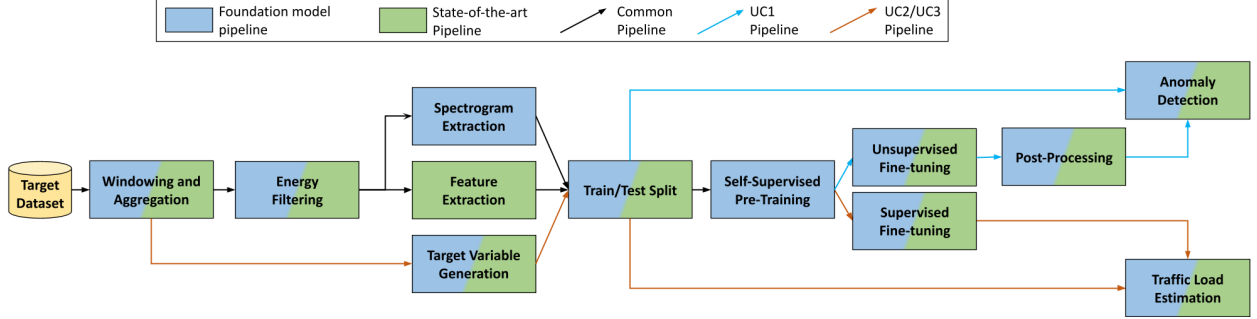


Figure 3: Overview of the processing pipeline for traffic load estimation and anomaly detection. In blue are the blocks for our foundation model pipeline, and in green are the ones for SoA algorithms. Both colours are used for shared blocks.

of the detected vehicle, its length, weight, speed, and the number of vehicle axles. The ground truth labels from the WiM are associated with data gathered by the sensors by applying a time offset equal to the distance between each sensor and the WiM system, divided by the vehicle’s speed.

**Dataset** We utilize two days of data to train and evaluate our algorithms. We use the first complete day’s data, spanning from 00.00 to 23.59, and covering a variety of traffic conditions, only as pre-training data for the foundation model. We then use the first half of the following day (00.00 to 12.00) as additional training data for supervised fine-tuning on this specific task. Finally, the last half day’s data is reserved for testing. It’s important to note that, in the 600 m between the WiM and the bridge, vehicle speeds may vary, with potential lane changes, vehicle overtaking, and overlapping. As a result, vibrations on the bridge may not be entirely correlated with the data collected from the WiM, which can unavoidably lead to a loss of accuracy in this analysis.

## 5 Methodology

This section presents our novel approach to vibration-based SHM leveraging self-supervised learning and Transformer foundation models. Firstly, we outline the data processing toolchain and train/test splitting (Section 5.1). Then, we delve into our model architecture (Section 5.2) and training strategies (Section 5.3). The core objective of our work is to understand whether it is possible to pre-train a large Transformer model on substantial amounts of unlabeled data and then fine-tune it to realize different SHM tasks. We consider both AD and TLE as downstream tasks to validate this hypothesis, focusing on all three Use Cases (UCs) described in Sec. 4. Specifically:

- AD is formulated as a “one-class” classification, discriminating between normal and anomalous structural states, similar to the approach of [36].
- TLE is framed as a regression problem, predicting a scalar traffic value. For UC2, we split the estimation of light and heavy vehicle traffic into two separate tasks.

### 5.1 Pre-processing Pipeline

The complete data processing pipeline used in our work is shown in Figure 3. This section outlines the pre-processing applied before inputting data into our masked autoencoder. The pre-processing settings are consistent for training and validation data across all analyzed UCs, except when expressly indicated.

The first pre-processing step is **windowing**, i.e., the division of the time-series data into time windows, which the algorithm can process. For UC1, we use 5s windows, as in the reference paper [36], with a stride of 2s to increase the number of training samples. For the other use cases, we enlarge the window to 60s since this dimension yields superior performance in the reference study [10], using a 2s stride in UC2, and 15s stride, given the very large data size, in UC3. All windows are composed of uni-dimensional signals since we always employ either a single sensor or multiple sensors, but consider them separately. We also only consider the z-axis of the acceleration data. Thus, each window is always a single vector of dimension  $T = 100 \times T_{win}$ , where 100 is the acceleration sampling frequency in all three datasets. All time windows are normalized with mean and standard deviation.

After creating the windows, we apply **energy filtering**, i.e., we disregard as irrelevant those windows whose cumulative energy is under a certain threshold,  $th = 3.125 \times (10^{-5})$  for UC1 and  $th = 1.25 \times 10^{-6}$  for UC2 and UC3. Energy

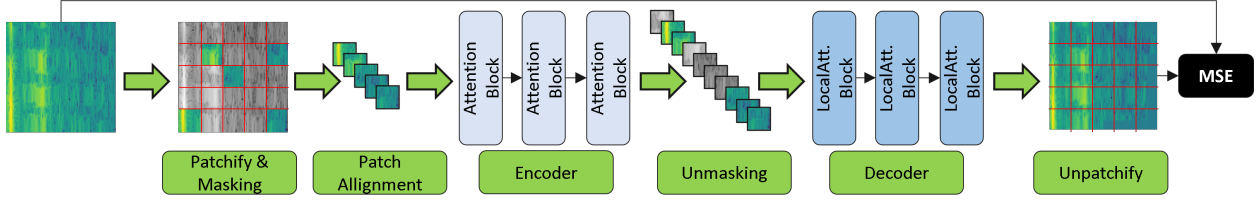


Figure 4: Architecture of our masked autoencoder during pre-training.

thresholds are computed using the iterative process proposed in [36]. Then, since masked autoencoders have been shown to reconstruct signals better in the frequency domain [17], the acceleration **spectrogram** is extracted. Precisely, we feed the model with 100x100 time-frequency representations in the form of spectrograms. The first dimension corresponds to the temporal domain, while the second captures the frequency domain. While we notice that this window is big enough to obtain good task performance, we did not explore the downscaling of the spectrogram image to reduce the models’ computational complexity, as the reduction of the input size has an impact only on the dimension of the last layer, whose size is negligible with respect to the whole model size.

For UC2 and UC3, we also need to generate the **target traffic variable**, while for UC1, samples are already separated between anomalous and normal based on time (see Sec. 4.1). Despite being generated differently for the two use cases, respectively from an optical camera and a WiM system, the target variables for UC2 and UC3 are identical. Namely, as described in [10], the target traffic load values for regression ( $y$ ) in UC2 are set to:

$$y = \frac{\sum_{t=1}^T (l_t = k)}{10} \quad (1)$$

where  $k = 1$  for light vehicles and  $k = 2$  for heavy vehicles, and  $\sum (l_t = k)$  indicates the number of samples that have label  $k$  in that window. Notice that  $y$  can also be a fractional number when the beginning/end of the window includes only a subset of a group of 10 consecutive samples sharing the same label. For UC3, the only difference is the lack of separation between light vehicles and heavy vehicles. After pre-processing, data are split between **train and test** as described in Section 4, and summarized in Table 1.

Lastly, we also apply a post-processing smoothing technique on the output of our trained model for UC1. Specifically, we label a window as anomalous or normal based on the *median* over a variable size set of consecutive predictions. Namely, we experiment with median filters over  $\{15, 30, 60, 120, 240\}$  consecutive windows.

## 5.2 Foundation Model Architecture

Our model architecture draws inspiration from the Masked Autoencoder proposed in [17], which was originally introduced to learn self-supervised representations from audio spectrograms. The model uses a stack of standard Transformer blocks for both the encoder and the decoder, each consisting of multiple attention layers. As a backbone, we use ViT-Base (ViT-B), but we simplify it by employing only three attention blocks for the encoder and decoder, drawing inspiration from the smallest option in [44]. The model takes as input acceleration spectrograms divided into non-overlapped regular grid patches, with a configurable portion of them being masked during training. The complete architecture is shown in Fig. 4.

To fine-tune our foundation model on the considered downstream tasks, architectural modifications are necessary. Namely, the model architecture remains unchanged when fine-tuning on UC1, because the task is framed as an outlier detection [36]: during training, the model learns the latent representation of normal data only, so that during testing, the decoder is expected to fail in accurately reconstructing data that deviates from its learned patterns. Accordingly, those samples whose reconstruction error (computed as detailed in Sec. 5.3.1) exceeds a user-defined threshold are classified as anomalies or outliers. On the other hand, the decoder is removed when fine-tuning on TLE tasks, and a single fully connected layer is appended directly to the latent representation produced by the encoder. The added layer has a single output neuron and is trained to predict the scalar target traffic variable defined in Eq. 1.

## 5.3 Training Phases

The training of our masked autoencoder involves two main phases. Namely, the model is first pre-trained considering data from all three datasets and then fine-tuned on each single task. The two phases are detailed in the following, distinguishing the fine-tuning procedure for UC1 (AD) and for UC2/3 (TLE). In both phases, we use an AdamW optimizer [45] with different learning rates based on the training phase. For the pre-training phase, we use a learning



rate of  $0.25 \cdot 10^{-3}$ , while for the fine-tuning phase a learning rate of  $0.25 \cdot 10^{-2}$  for UC1,  $0.25 \cdot 10^{-5}$  for UC2 and UC3, and a weight decay of 0.05. Following what was presented in [44, 46], we apply automatic gradient scaling to avoid exploding gradients. During pre-training, we also progressively increase the learning rate from 0 to the pre-training learning rate value over the first 100 epochs to improve the convergence. After this, the learning rate is reduced following the half-cycle of the cosine function. We pre-train our foundation model for 200 epochs with a batch size of 128, then fine-tune it for 400, 500, and 200 epochs with batches of 64, 8, and 128 samples on UC1, UC2, and UC3, respectively.

### 5.3.1 Pre-training

The full encoder-decoder model, with the architecture of Fig. 4 is initially pre-trained on a large amount of unlabeled data. We select pre-training data following the split described Section 2, combining the *training sets of all three UCs*. Note that, although our data have labels, we do not use them in this phase, to simulate a scenario where the costly process of labelling all available samples is not affordable.

During pre-training, the non-overlapping spectrogram patches of each input sample are masked with probability  $p = 0.8$  (masking ratio) and aligned, before being passed to the transformer encoder. The latter then processes the non-masked patches to produce latent representations. Encoded patches are padded with trainable mask tokens and fed to the decoder, whose objective is to reconstruct the original spectrogram, including the missing parts. The encoder and decoder are jointly optimized to minimize the Mean Squared Error (MSE) between the reconstruction and the input spectrogram, averaged over masked patches. This pre-training is completely self-supervised and task-independent. Its objective is to learn robust latent representations of SHM data that allow the model to infer the underlying patterns in the data despite the missing information.

### 5.3.2 Fine-tuning

The details of the fine-tuning phase differ depending on the downstream task. For UC1 (AD), as mentioned above, we maintain the autoencoder structure of our model and use a threshold on the reconstruction error to identify anomalies. Therefore, since the fine-tuning architecture is the same as pre-training, the model is further trained in an unsupervised way using the same procedure just described, but considering only normal data from the UC1 dataset.

For UC2, the pre-trained model is fine-tuned considering the 21 minutes of coupled acceleration data and video recording on the viaduct presented in Sec. 4.2.1. Two separate fine-tunings are executed for light and heavy vehicle TLEs, starting from the same pre-trained model. For UC3, we consider the first half of the second day’s data to fine-tune our foundation model, as described in 4.2.2. For these two downstream tasks, we follow a classic supervised fine-tuning procedure, where the model learns to predict the traffic load values rather than to reconstruct the input spectrograms. As a loss function, we use the MSE between the newly inserted fully connected layer’s output prediction and the ground truth target variable.

## 5.4 Model Size Exploration and Knowledge Distillation

We carry out an extensive search on the optimal size of our foundation models. To this end, we systematically decrease the embedding dimensions of both the encoder and the decoder from the baseline dimensions  $(e_{dim}, d_{dim}) = (768, 512)$  scaling them progressively by a factor 2 down to  $(e_{dim}, d_{dim}) = (24, 16)$ . These new models are pre-trained on all datasets and subsequently fine-tuned on the three downstream tasks, following the same procedure described in the previous section. Additionally, we considered a modified fine-tuning procedure enhanced with Knowledge Distillation (KD). In this setup, considering the baseline model as a teacher, the student utilizes a multi-objective fine-tuning loss function composed of two contributions: the first one,  $\mathcal{L}_{task}$ , is the Mean Absolute Error (MAE) computed on student prediction against the ground truth, while the second one,  $\mathcal{L}_{KD}$ , is the Root Mean Squared Error (RMSE) between student and teacher predictions. Through an empirical approach, we assessed that evenly balancing these two contributions leads to faster convergence of the overall loss, whose function becomes:

$$\mathcal{L} = 0.5 \cdot \mathcal{L}_{task}(y_s, y_{true}) + 0.5 \cdot \mathcal{L}_{KD}(y_s, y_t) \quad (2)$$

where  $y_s$ ,  $y_t$ , and  $y_{true}$  are the student, the teacher, and the true predictions, respectively. Even when using KD in fine-tuning, for all UCs, student models are always first pre-trained following the self-supervised procedure of Sec. 5.3.1.

## 6 Results

In this section, we first introduce our comparison baselines and then detail the results of our foundation models on the three use cases. We also quantify the impact of self-supervised pre-training on the performance of our models. Lastly,

Table 2: Models employed in our experiments.

Model	Task	Hyperparameters
State-of-the-art		
LR	TLE	-
RF	TLE	Depth = 200, Trees = 30
k-NN	TLE	k = 7
MLP	TLE	Layers = 3, Neurons = 100
SVR	TLE	Kernel = RBF, C = 10.0, $\epsilon=0.1$
PCA	AD	CF = 32
Our Work		
Masked autoencoder	TLE, AD	See Section 5

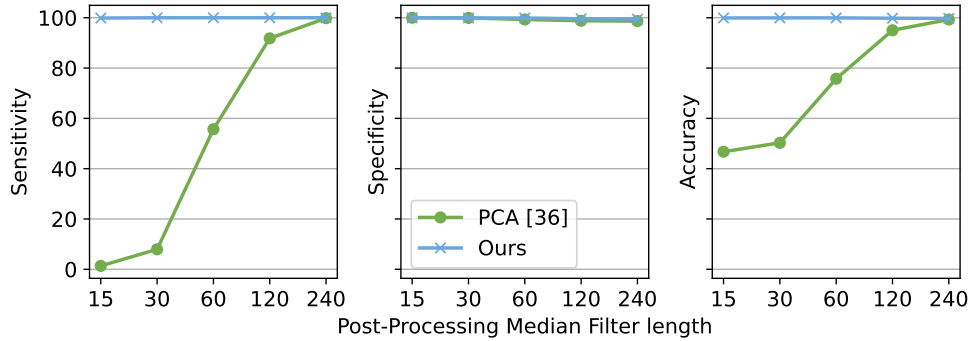


Figure 5: SoA PCA [36] vs. masked autoencoder performance while varying the smoothing post-processing median filter length.

we analyze the trade-off between model size and performance and compare regular and KD-enhanced fine-tuning. In all experiments except the last one, we consider our largest masked autoencoder version, i.e.,  $(e_{dim}, d_{dim}) = (768, 512)$ .

## 6.1 Comparison Baselines

For UC1, we compare against the top-performing model of [36], a PCA that considers a window dimension of 5 seconds (500 samples at 100 Hz) and a post-processing median filter with varying length to aggregate consecutive predictions.

For UC2 and UC3, we compare with the five supervised algorithms proposed in [10], i.e., the work that first introduced the UC2 dataset. Namely, we consider: i) a K-Nearest Neighbors (k-NN); ii) a Linear Regressor (LR); iii) a Random Forest (RF) trained with the variance reduction criterion [47]; iv) a Support Vector Regressor (SVR); v) a Multi-Layer Perceptron (MLP) with ReLU activations, trained with the *Adam* optimizer, a learning rate of  $10^{-3}$  and a mini-batch size of 200. A summary of the state-of-the-art models and their hyperparameters is shown in Table 2.

## 6.2 Anomaly Detection (UC1) Results

We evaluate AD models in terms of *specificity*, computed as the correctly classified normal windows, *sensitivity*, i.e., the correctly classified anomalous windows, and *accuracy*, i.e., the ratio of correctly classified windows overall. For both our models and the baseline PCA, we use the same procedure of [36] to determine the reconstruction error threshold associated with anomalies. Namely, the threshold is initialized to the average MSE on normal (training) data, to which we add the standard deviation over a single day of normal data. The value is then progressively increased by a small step until 100% specificity is achieved on this single validation day.

Figure 5 shows the comparative performance of PCA and our foundation model while varying the number of windows' outputs fed to the median filter as post-processing. The graph highlights the increasing trend of accuracy, sensitivity, and specificity as the dimension increases for both methods. However, we can observe a significant improvement in all evaluation metrics of our model compared to the PCA, especially for short time windows. For example, when applying the median smoothing to 60 windows, our masked autoencoder achieves an accuracy of 99.92%, while the PCA only reaches 75.76%. To match the accuracy of our model, the PCA needs a post-processing median filter of 240 windows,

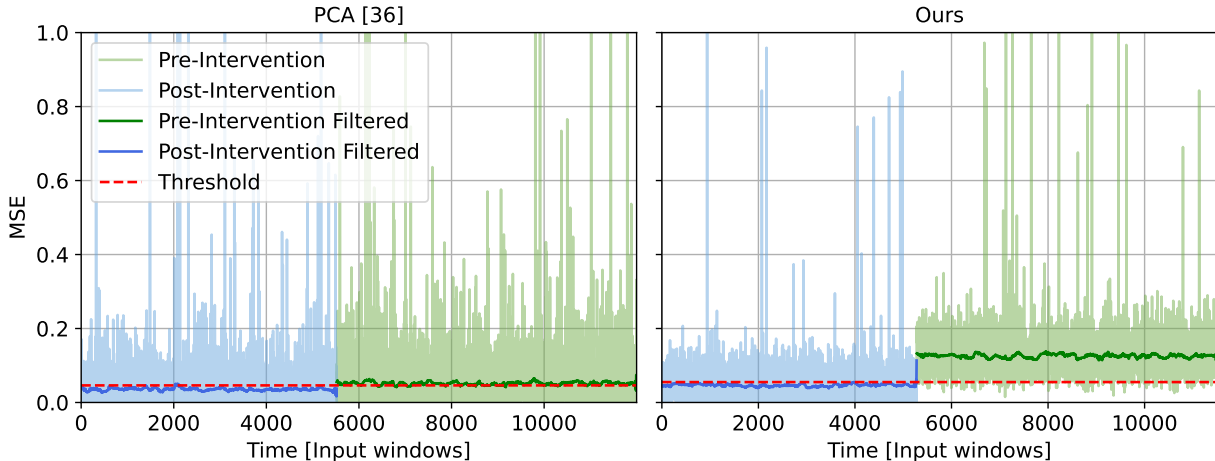


Figure 6: Reconstruction error of the PCA [36] and our proposed model, for normal and anomalous windows

Table 3: Comparison between the algorithms of [10] and the masked autoencoder proposed in our work on UC2. The comparison uses the features extraction of [10] for the baselines and raw data for our method. Bold = best result, underline = second best.

Model	Heavy Vehicles					Light Vehicles				
	MSE	MAE	$R^2$	MSE%	MAE%	MSE	MAE	$R^2$	MSE%	MAE%
	State-of-the-art									
SVR	<u>0.35</u>	0.42	<u>0.91</u>	<u>10.76</u>	12.85	2.23	1.05	0.76	37.03	17.50
RF	0.38	<u>0.32</u>	0.91	11.76	<u>9.66</u>	<u>1.50</u>	<b>0.73</b>	<u>0.84</u>	<u>25.02</u>	<b>12.10</b>
MLP	0.53	<u>0.53</u>	0.87	16.37	16.37	2.99	1.35	0.67	49.69	22.44
kNN	0.37	0.41	0.91	11.47	12.45	2.26	1.09	0.75	37.59	18.14
LR	1.19	0.84	0.71	36.57	25.82	7.34	2.14	0.20	121.94	35.67
	Our Work									
Masked Autoencoder	<b>0.11</b>	<b>0.25</b>	<b>0.97</b>	<b>3.42</b>	<b>7.88</b>	<b>0.95</b>	<b>0.75</b>	<b>0.90</b>	<b>15.92</b>	<b>12.44</b>

i.e., 4x larger. The sensitivity shows a similar trend: for a 60-windows smoothing, our model reaches 99.9%, compared to 55.68% of the PCA.

Having a shorter post-processing median filter translates into a significantly lower anomaly detection latency. For example, given that each window is 5s long, a median filter over 240 windows, as required by the PCA, corresponds to a latency of 20 minutes before an anomaly can be signalled. In contrast, our method reduces this latency to 5 minutes.

Additionally, the specificity values demonstrate the masked autoencoder’s superiority in correctly identifying normal data instances. We achieve an almost perfect specificity (min. 99.97%) for all time window dimensions, whereas PCA shows lower specificity values, ranging from 96.21% to 99.87%.

To visualize the performance of our model compared to the PCA, Figure 6 shows the reconstruction error (MSE) of normal and anomalous windows. The darker line shows the output of median-smoothing over 120 windows. From the figure, we can notice that the PCA reconstruction error is more noisy, and, after the smoothing post-processing, it shows a very small margin between normal and anomalous signals. On the other hand, our approach shows a much more pronounced difference between pre and post-intervention data, thus being able to more robustly tell apart normal and anomalous windows.

### 6.3 Traffic Load Estimation (UC2 and UC3) Results

To compare the performance of TLE models, we consider 5 different metrics: MSE, MAE,  $R^2$  score, Mean Squared Percentage Error (MSE%) and Mean Absolute Percentage Error (MAE%), where the last two are obtained dividing the MSE and MAE by the average predicted value on the test set, allowing to quantify the error magnitude w.r.t. the true values.

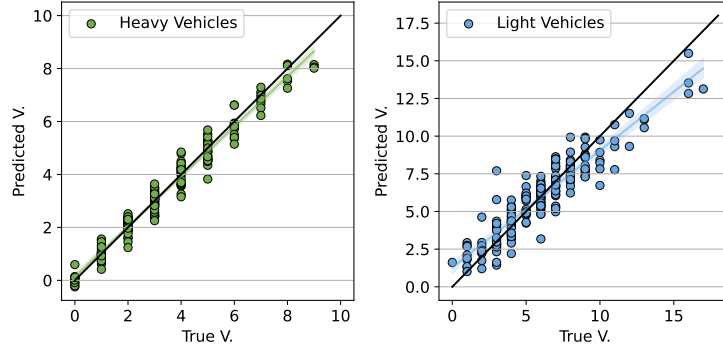


Figure 7: True vs predicted values of the TLE regression task for heavy and light vehicles. The black line represents the ideal prediction (true value = predicted value). The coloured straight lines are the linear interpolation of the predicted samples, and the light-coloured area corresponds to the 99.5% confidence interval of the interpolation.

Table 4: Comparison between the algorithms of [10] and the masked autoencoder proposed in our work on the UC3. The comparison uses all the extracted features for the baselines and raw data for the masked autoencoder.

Model	MSE	MAE	$R^2$	MSE%	MAE%
State-of-the-art					
LR	20.53	2.05	-14.40	1091.02	109.03
RF	2.23	1.10	-0.67	118.48	58.30
kNN	1.34	0.90	-0.01	71.14	47.81
MLP	<u>1.20</u>	<u>0.85</u>	<u>0.10</u>	<u>63.89</u>	<u>45.39</u>
SVR	1.39	0.91	-0.04	73.77	48.19
Our Work					
Masked Autoencoder	<b>0.62</b>	<b>0.57</b>	<b>0.54</b>	<b>32.93</b>	<b>30.13</b>

### 6.3.1 UC2

Table 3 reports the results obtained on UC2 for light and heavy vehicles. Considering the latter, we outperform the best baseline models from [10] (SVR and RF) in all metrics. However, our foundation model reduces the MSE by 3.2x, the MAE by 1.3x, and improves the  $R^2$  of +0.06. We impute this to the increased capacity of our foundation model, which permits to better leverage the non-linear and higher-order interactions within acceleration data that correlate with traffic flow, while current SoA machine learning methods exhibit limitations in capturing these intricate relationships. Additionally, notice how there is no single best SoA model, while our approach convincingly overcomes them all in every considered metric. For the prediction of the light vehicle traffic, our foundation model outperforms the SoA in terms of MSE (1.6x reduction) and  $R^2$  (+0.06) and is the second best in terms of MAE (1.03x increase over the best baseline model, the RF). Importantly, having a significantly lower MSE and a slightly higher MAE means that our approach does not output predictions that are far off the ground truth, as the quadratic function of the MSE penalizes major mistakes. Thus, it could be more amenable for a real-world deployment than the baseline RF.

Figure 7 plots the ground truth target variable against our model’s predictions to further highlight our approach’s effectiveness. As shown, most predictions are close to the target without noticeable outliers. The black line represents the ideal prediction, where true values exactly correspond to the predicted values. The coloured straight lines correspond to the linear interpolation of the predicted samples, while the light-coloured area corresponds to the 99.5% confidence interval of the interpolation. For the heavy vehicle case, the confidence interval almost overlaps with the ideal prediction across traffic conditions (i.e., x-axis values), further validating the effectiveness of our approach in this scenario. For light vehicles, when facing high traffic, the model’s confidence interval slightly deviates from the ideal prediction, underestimating the traffic on the viaduct. This may be a consequence of the lower weight of light vehicles. The latter generate vibrations with lower amplitudes on the viaduct, where vibrations caused by multiple vehicles can be easily mistaken for a single vehicle in light traffic. Further, the model is biased towards lower-value TLE estimations, given the scarcity of high-traffic window samples.

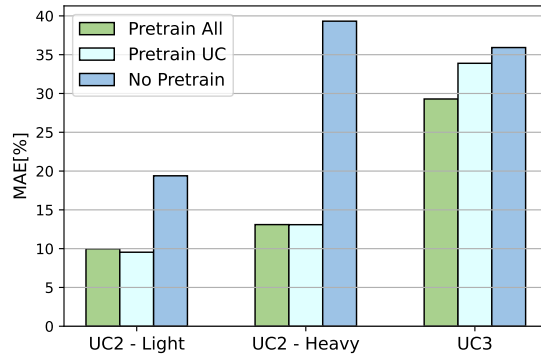


Figure 8: Impact of different pre-trainings on masked autoencoder outcome.

### 6.3.2 UC3

The results of UC3 are shown in Table 4. We compare our approach with the same models considered for UC2. However, since there is no previous literature on this dataset, we re-train all baseline models with the same data split used for our foundation model while keeping the same hyper-parameter settings of [10]. Results show that our foundation model overcomes state-of-the-art performance on all metrics. The second-best performing model, the MLP, fails to reach acceptable results, demonstrating the higher complexity of this UC. Our fine-tuned foundation model can decrease the MSE and MAE of the MLP by  $1.9\times$  and  $1.5\times$ , respectively, while increasing the  $R^2$  score by  $5.4\times$  as well.

It is worth noticing that this is the task with the largest dataset available for training: this could further explain the superiority of our approach, which is expected to thrive when more data are available, and, at the same time, justify the limits of SoA approaches, as their shallow nature may be unsuited to handle this complexity. The observed performance degradation for both state-of-the-art and our proposed approaches on UC3 compared to UC2 can be attributed to two key factors. Firstly, sensor placement may be a factor influencing task difficulty. In fact, unlike UC2, sensors are positioned on two external beams per span, which might lead to reduced sensitivity to vehicle-induced vibrations. Secondly, as anticipated in Section 4, the label assignment procedure likely introduces noise into the training data. The physical separation of the WiM system from the bridge disrupts the correlation between bridge vibrations and WiM collected data. While the model might be accurately predicting traffic load based on the collected data, the ground truth labels assigned based on the WiM system may not accurately reflect real-world bridge behaviour. This misalignment between predicted and actual bridge conditions may partially explain the performance drop observed on this use case.

## 6.4 Impact of pre-training

In this section, we demonstrate that self-supervised pre-training is a fundamental contributor to the performance of our foundation models. Considering UC2 and 3, we apply three different training setups:

- **No Pretrain:** the pre-training step is completely disregarded, and the model is directly trained in a supervised way considering only UC-specific data;
- **Pretrain UC:** the model is first pre-trained and then fine-tuned only considering data of the specific use case. Thus, the *same training data* are applied during the masked autoencoder self-supervised pre-training training and during supervised fine-tuning (after replacing the decoder with the classification head);
- **Pretrain All:** the model is pre-trained on all three datasets (combining the respective training sets) and fine-tuned on UC-specific data.

The test MAE% obtained by our foundation model in the three cases are reported in Figure 8. As shown, *No Pretrain* always performs worse than the other two setups, underlying the usefulness of self-supervised pre-training. Quantitatively, *Pretrain All* reduces the MAE% by  $1.94\times$ ,  $3\times$  and  $1.2\times$  on UC2-Light, UC2-Heavy and UC3, respectively, compared to *No Pretrain*. As expected, the benefits of pre-training are more evident for UC2, which has the smallest dataset. Moreover, pre-training the foundation model on all three datasets shows the best results for UC3 (with *Pretrain All* achieving  $1.2\times$  lower MAE% compared to *Pretrain UC*), while no clear advantage is evident for UC2. This is in accordance with the observation of the previous section that UC3 is the most difficult downstream tasks among the three, thus benefitting more from high-quality and generalizable representations. These findings indicate

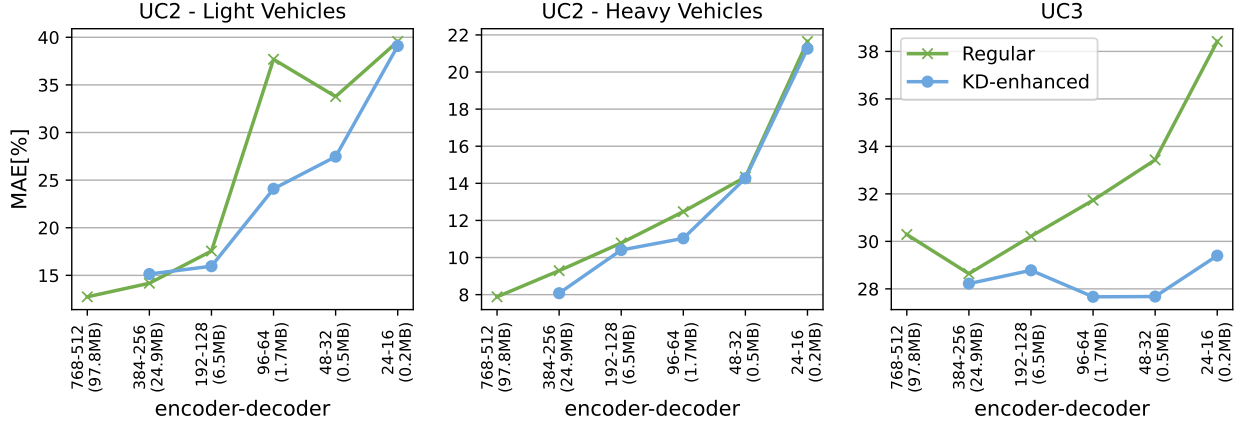


Figure 9: MAE% comparison between regular and KD-enhanced fine-tuning.

that the effectiveness of this approach might be further amplified by leveraging substantially larger and more diverse datasets for pre-training.

## 6.5 Model size optimization and Knowledge Distillation

We analyze the trade-off between model size and performance. For all UCs, following the findings of the previous section, we use a *Pretrain All* scheme, and we compare how regular supervised fine-tuning stands against KD-enhanced fine-tuning. We focus on TLE tasks because, for UC1, we were able to obtain the same performance shown in Figure 5 for the largest transformer, with a model of just 0.2MB, with  $(e_{dim}, d_{dim}) = (24, 16)$ . Results for UC2 and UC3 are shown in Figure 9. For clarity’s sake, we present results only in terms of MAE%, as other metrics follow similar trends. As shown, KD helps improve the performance of the models in almost all configurations, with the exception of a few cases related to UC2, especially in the low-size regime, where it provides marginal advantages. This is motivated by the fact that student networks that are too small cannot imitate the predictions of much larger teachers. Hence, the KD loss only adds noise to the training signal. At most, on UC2, KD improves the MAE by  $1.6\times$  on light vehicles, at  $(e_{dim}, d_{dim}) = (96, 64)$ , and by  $1.15\times$  on heavy vehicles, at  $(e_{dim}, d_{dim}) = (384, 256)$ , compared to regular fine-tuning. In the latter case, the KD-enhanced model reaches a MAE% that is just  $1.2\times$  higher than the teacher while being  $3.9\times$  smaller.

The most interesting results are obtained on UC3. Here, we first note that reducing the model size to  $(e_{dim}, d_{dim}) = (384, 256)$  is beneficial for performance (5% reduction for a  $3.9\times$  smaller size) even without KD. Moreover, we can achieve very competitive results even with smaller models thanks to our KD-enhanced fine-tuning setup, which is very effective. The most interesting result is achieved at  $(e_{dim}, d_{dim}) = (48, 32)$ , which further reduces the MAE% by 8.6% compared to the baseline, with a model whose parameters only require 0.5MB, i.e.,  $195\times$  smaller than the original one.

These results show the effectiveness of KD in reducing model size while preserving as much as possible the performance of foundation models from the perspective of real-world deployment resource-constrained devices. The two smallest student configurations require less than 0.7 MBs and could be deployed on the data collection nodes mentioned in Section 4, which are equipped with 1 MB of Flash memory. However, it must be underlined that, on UC2, these downsized models remain hindered by performance gaps that might be too large depending on application-specific requirements. Further research is necessary to bridge these gaps, but we believe that our results show promise in the direction of achieving tiny embodied foundation models for SHM.

## 7 Conclusions

We proposed a task-independent foundation model for SHM applications, which can achieve state-of-the-art performance on two tasks, Anomaly Detection and Traffic Load Estimation, considering three different datasets. Our transformer-based masked autoencoder learns powerful representations of vibration data gathered by accelerometers during the pre-training step and can be then effectively fine-tuned on the specific downstream task. We believe that our work points to a new and exciting direction in ML for SHM research. Future works may include using a larger and more diverse pre-training dataset, as our results already suggested this could lead to possible benefits, as well as experimenting more thoroughly with model hyper-parameters.

## 8 Acknowledgment

This publication is part of the project PNRR-NGEU which has received funding from the MUR – DM 117/2023. We thank Sacertis Ingegneria Srl for providing the data for this research.

## References

- [1] G. T. Webb *et al.*, “Analysis of fiber-optic strain-monitoring data from a prestressed concrete bridge,” *Journal of Bridge Engineering*, vol. 22, no. 5, p. 05017002, 2017.
- [2] E. Odat *et al.*, “Vehicle classification and speed estimation using combined passive infrared/ultrasonic sensors,” *IEEE transactions on intelligent transportation systems*, vol. 19, no. 5, pp. 1593–1606, 2017.
- [3] H. Liu *et al.*, “Vehicle detection and classification using distributed fiber optic acoustic sensing,” *IEEE Transactions on Vehicular Technology*, vol. 69, no. 2, pp. 1363–1374, 2019.
- [4] Z. Ye *et al.*, “Collecting comprehensive traffic information using pavement vibration monitoring data,” *Computer-Aided Civil and Infrastructure Engineering*, vol. 35, no. 2, pp. 134–149, 2020.
- [5] C.-H. Lin *et al.*, “A real-time bridge structural health monitoring device using cost-effective one-axis accelerometers,” in *2015 IEEE Tenth International Conference on Intelligent Sensors, Sensor Networks and Information Processing (ISSNIP)*, 2015, pp. 1–2.
- [6] A. Hashad, “Using dynamic analysis of site vibration to select the suitable vibration limit,” *HBRC Journal*, vol. 14, no. 2, pp. 180–188, 2018.
- [7] S. Kamkar and R. Safabakhsh, “Vehicle detection, counting and classification in various conditions,” *IET Intelligent Transport Systems*, vol. 10, no. 6, pp. 406–413, 2016.
- [8] V. Shahsavari *et al.*, “Diagnostic testing of a vertical lift truss bridge for model verification and decision-making support,” *Frontiers in Built Environment*, vol. 5, 2019.
- [9] E. Parisi *et al.*, “Time and frequency domain assessment of low-power mems accelerometers for structural health monitoring,” in *2022 IEEE International Workshop on Metrology for Industry 4.0 & IoT (MetroInd4.0&IoT)*, 2022, pp. 234–239.
- [10] A. Burrello *et al.*, “Traffic load estimation from structural health monitoring sensors using supervised learning,” *Sustainable Computing: Informatics and Systems*, vol. 35, p. 100704, 2022.
- [11] R. P. Finotti *et al.*, “An shm approach using machine learning and statistical indicators extracted from raw dynamic measurements,” *Latin American Journal of Solids and Structures*, 2019.
- [12] S.-Y. Kim and M. Mukhiddinov, “Data anomaly detection for structural health monitoring based on a convolutional neural network,” *Sensors*, vol. 23, p. 8525, 2023.
- [13] K. Yang *et al.*, “Unsupervised long-term damage detection in an uncontrolled environment through optimal autoencoder,” *Mechanical Systems and Signal Processing*, vol. 199, p. 110473, 2023.
- [14] E. M. Coraça *et al.*, “An unsupervised structural health monitoring framework based on variational autoencoders and hidden markov models,” *Reliability Engineering & System Safety*, vol. 231, p. 109025, 2023.
- [15] N. Römgens *et al.*, “On using autoencoders with non-standardized time series data for damage localization,” *Engineering Structures*, vol. 303, p. 117570, 2024.
- [16] R. Wang *et al.*, “A novel transformer-based semantic segmentation framework for structural condition assessment,” *Structural Health Monitoring*, vol. 23, no. 2, pp. 1170–1183, 2024.
- [17] P.-Y. Huang *et al.*, “Masked autoencoders that listen,” *Advances in Neural Information Processing Systems*, vol. 35, pp. 28 708–28 720, 2022.
- [18] R. Bommasani, P. Liang *et al.*, “On the opportunities and risks of foundation models,” *ArXiv*, 2021.
- [19] Y. Yu *et al.*, “State-of-the-art review on bridge weigh-in-motion technology,” *Advances in Structural Engineering*, vol. 19, no. 9, pp. 1514–1530, 2016.
- [20] A. Vaswani *et al.*, “Attention is all you need,” in *Advances in Neural Information Processing Systems*, I. Guyon, U. V. Luxburg, S. Bengio, H. Wallach, R. Fergus, S. Vishwanathan, and R. Garnett, Eds., vol. 30, 2017.
- [21] E. Wang *et al.*, “Multi-modal knowledge graphs representation learning via multi-headed self-attention,” *Information Fusion*, vol. 88, pp. 78–85, 2022.

- [22] A. Dosovitskiy *et al.*, “An image is worth 16x16 words: Transformers for image recognition at scale,” *ArXiv*, 2021.
- [23] K. He *et al.*, “Masked autoencoders are scalable vision learners,” in *2022 IEEE/CVF Conference on Computer Vision and Pattern Recognition (CVPR)*, 2022, pp. 15 979–15 988.
- [24] G. Paaß and S. Giesselbach, “Foundation models for natural language processing – pre-trained language models integrating media,” *ArXiv*, 2023.
- [25] L. Yuan *et al.*, “Florence: A new foundation model for computer vision,” *ArXiv*, 2021.
- [26] X. Sun *et al.*, “Dime-fm : Distilling multimodal and efficient foundation models,” in *2023 IEEE/CVF International Conference on Computer Vision (ICCV)*, 2023, pp. 15 475–15 487.
- [27] J. A. Miller *et al.*, “A survey of deep learning and foundation models for time series forecasting,” *ArXiv*, 2024.
- [28] M. Goswami *et al.*, “Moment: A family of open time-series foundation models,” *ArXiv*, 2024.
- [29] D. Lydon *et al.*, “Use of a roving computer vision system to compare anomaly detection techniques for health monitoring of bridges,” *Journal of Civil Structural Health Monitoring*, vol. 12, no. 6, pp. 1299–1316, 2022.
- [30] C. Zhao *et al.*, “Uav dispatch planning for a wireless rechargeable sensor network for bridge monitoring,” *IEEE Transactions on Sustainable Computing*, vol. 8, no. 2, pp. 293–309, 2023.
- [31] O. Abdeljaber *et al.*, “Real-time vibration-based structural damage detection using one-dimensional convolutional neural networks,” *Journal of Sound and Vibration*, vol. 388, pp. 154–170, 2017.
- [32] L. Zanatta *et al.*, “Damage detection in structural health monitoring with spiking neural networks,” in *2021 IEEE International Workshop on Metrology for Industry 4.0 & IoT (MetroInd4. 0&IoT)*, 2021, pp. 105–110.
- [33] F. Barchi *et al.*, “Spiking neural network-based near-sensor computing for damage detection in structural health monitoring,” *Future Internet*, vol. 13, no. 8, p. 219, 2021.
- [34] J. Liu *et al.*, “Diagnosis algorithms for indirect structural health monitoring of a bridge model via dimensionality reduction,” *Mechanical Systems and Signal Processing*, vol. 136, p. 106454, 2020.
- [35] K. A. Eltouny and X. Liang, “Large-scale structural health monitoring using composite recurrent neural networks and grid environments,” *Computer-Aided Civil and Infrastructure Engineering*, vol. 38, no. 3, pp. 271–287, 2023.
- [36] A. Moallemi *et al.*, “Exploring scalable, distributed real-time anomaly detection for bridge health monitoring,” *IEEE Internet of Things Journal*, vol. 9, no. 18, pp. 17 660–17 674, 2022.
- [37] H. Dong *et al.*, “Improved robust vehicle detection and identification based on single magnetic sensor,” *Ieee Access*, vol. 6, pp. 5247–5255, 2018.
- [38] Q. Wang *et al.*, “Roadside magnetic sensor system for vehicle detection in urban environments,” *IEEE Transactions on Intelligent Transportation Systems*, vol. 19, no. 5, pp. 1365–1374, 2017.
- [39] A. Boukerche, D. Zhong, and P. Sun, “Feco: An efficient deep reinforcement learning-based fuel-economic traffic signal control scheme,” *IEEE Transactions on Sustainable Computing*, vol. 7, no. 1, pp. 144–156, 2022.
- [40] A. Ferguson *et al.*, “Detecting vehicle loading events in bridge rotation data measured with multi-axial accelerometers,” *Sensors*, vol. 22, p. 4994, 2022.
- [41] A. Burrello *et al.*, “Enhancing structural health monitoring with vehicle identification and tracking,” in *2020 IEEE International Instrumentation and Measurement Technology Conference (I2MTC)*, 2020, pp. 1–6.
- [42] “lis344alh sensor, STMicroelectronics.”
- [43] “Hts221 sensor, STMicroelectronics.”
- [44] H. Touvron *et al.*, “Training data-efficient image transformers & distillation through attention,” in *International Conference on Machine Learning*, vol. 139, 2021, pp. 10 347–10 357.
- [45] I. Loshchilov and F. Hutter, “Decoupled weight decay regularization,” *ArXiv*, 2019.
- [46] H. Bao *et al.*, “BEit: BERT pre-training of image transformers,” in *International Conference on Learning Representations*, 2022.
- [47] L. Breiman *et al.*, *Classification and regression trees*. Wadsworth & Brooks/Cole Advanced Books & Software, 1984.